https://doi.org/10.46813/2024-152-054

UDC 539.53:691.714

EFFECT OF SEVERE PLASTIC DEFORMATION AT HIGH TEMPERATURE ON THE MICROSTRUCTURE AND MECHANICAL PROPERTIES OF FERRITIC-MARTENSITIC STEEL T91

H.Yu. Rostova[1], I.V. Kolodiy[2], R.L. Vasilenko[2], O.S. Kalchenko[2], M.A. Tikhonovsky[2], O.M. Velikodnyi[2], G.D. Tolstolutska[2], V.S. Okovit[2]

[1]Institute of Fluid-Flow Machinery of the Polish Academy of Sciences, Gdańsk, Poland;

[2]National Science Center "Kharkov Institute of Physics and Technology", Kharkiv, Ukraine

E-mail: hrostova03@gmail.com

The microstructure and mechanical properties of ferritic-martensitic steel T91 after severe plastic deformation (SPD) and subsequent annealing (tempering) have been studied. The SPD of steel T91 was carried out by the method of multiple "upsetting-extrusion" at a temperature of 875 °C, subsequent annealing was carried out in the temperature range of 550...650 °C for 1…100 h. It has been found that the multiple "upsetting-extrusion" process allows the formation of an ultra-fine grained structure with an average grain size of 100 nm, which remains stable at the annealing temperatures of 550 and 600 °C for up to 100 h of exposure. After annealing at these temperatures, the microhardness remains at the level 3100 MPa and 2780 MPa, respectively, which is noticeably higher than with standard N&T heat treatment of this steel (2480 MPa). The refining and uniform distribution of MX-type carbide precipitates, due to severe plastic deformation, also leads to an increase in strength characteristics during tensile tests at temperatures of 20 and 600 °C.

INTRODUCTION

The issue of reactor energy efficiency is of great importance in the context of nuclear power, particularly in relation to the limited burn-up of nuclear fuel. In response to this challenge, the U.S. Department of Energy launched the Generation-IV Initiative in 2000. This program aims to expand the use of nuclear energy through further progress in the design of nuclear power systems [1]. The program resulted in a proposal for the research, development, and further implementation of six types of nuclear reactors of the future, the fourth generation (so-called "Gen-IV"). These reactors will have improved safety and reliability, sustainability, a lifetime of the reactor exceeding 60 years, and profitability. However, the Gen-IV power systems are designed to operate under more severe conditions than currently used reactors. These include higher core temperatures, higher neutron doses, and an extremely aggressive environment [2]. In this regard, there is an urgent need to develop new structural materials, since current steels and alloys are not suitable for operation in such harsh conditions [3, 4].

Chromium ferritic-martensitic steels with a composition of 9…12% are regarded as potential structural materials for Generation-IV reactors. These materials demonstrate an acceptable degree of resistance to neutron irradiation, and they exhibit a reduced tendency to swell in comparison to austenitic steels that are currently in use in present-day reactors [5–8]. The advantages of 9% Cr steels over 12% Cr steels include a lower tendency to form δ ferrite, which affects the creep and impact strength characteristics of steels, as well as a lower degree of low-temperature radiation embrittlement. However, 9%Cr steels also exhibit a notable disadvantage in their low high-temperature strength, which limits the maximum operating temperature to approximately 500 °C [4]. The primary method for overcoming this issue is thermomechanical treatment (TMT), in addition to alloying with elements that form high-melting carbides (VC, NbC, WC, etc.). This approach not only enhances the material's high-temperature mechanical characteristics, but it also increases its radiation resistance [4, 8]. Thermomechanical treatment enables the regulation of grain and subgrain dimensions, dislocation density, the type, density, and characteristics of the spatial distribution of carbide phases, which positively impacts the strength and plastic properties of steels across a broad range.

The standard heat treatment of heat-resistant ferritic-martensitic steels is normalizing and subsequent high-temperature tempering (commonly referred to as the N&T condition) [9]. The process of normalization entails austenitizing the material at a temperature exceeding the critical point A_{C1}, followed by cooling in air. For steels with 9% Cr, this treatment results in the formation of tempered martensite (BCT structure) [5, 10–12]. The austenitizing temperature for steels of this class should be sufficiently high to completely dissolve carbides while remaining sufficiently low to avoid the formation of δ-ferrite (a high-temperature modification of the BCC phase), which is retained during cooling. As shown in reference [13], the normalization of 9% chromium steels at 980 and 1180 °C results in the formation of 100% martensite, whereas steels quenched from 1280 °C contain approximately 20% δ-ferrite.

Nevertheless, the standard heat treatment of 9%Cr steels results in the formation of a coarse-grained structure with an average grain size of ~20…25 μm. It is reasonable to posit that a notable enhancement in

mechanical properties may be anticipated when an ultra-fine grained or nanostructured state is achieved in steel. This, in turn, may lead to an increase in the radiation resistance of the material, as evidenced by prior research [14–16]. The formation of this microstructure is achievable through the implementation of TMT in combination with severe plastic deformation (SPD), which can be achieved through a range of techniques [17–19].

One of the most frequently employed techniques in TMT is hot deformation within the austenite temperature range, which is designated as "ausforming". This treatment effectively increases the strength characteristics of steels by modernizing the microstructure. The objective of the study [20] was to examine the influence of a series of thermomechanical treatments, including warm-rolling in a metastable austenite phase, on the microstructure and properties of a commercially modified 9Cr-1Mo (G91) steel alloy. The samples produced via warm-rolling and subsequent tempering of the G91 alloy demonstrated a higher microhardness than the as-received, reference G91 alloy. The results of the ongoing creep tests indicated a significant increase in creep lifetime, with a factor exceeding 14. Furthermore, the tensile tests revealed a notable enhancement of the yield stress and ductility [20]. A number of studies [21–23] have demonstrated that high-temperature TMT of 9% Cr ferritic-martensitic steels results in a qualitative increase in their high-temperature strength.

In this context, the objective of this research is to investigate the impact of severe plastic deformation at high temperature on the microstructure and mechanical properties of ferritic-martensitic steel T91. To carry out SPD, we used the method of "multiple upsetting-extrusion" (MUE), which was previously used to refine the microstructure of T91 steel by deformation in the region of stability of the ferrite phase [24].

1. MATERIALS AND INVESTIGATION METHODS

T91 steel was produced by INDUSTELL, Belgium (melting: 504/3, heat 82566-4). Chemical composition of steel according to the manufacturer data is the follows: wt.%: 0.09 C; 8.76 Cr; 0.86 Mo; 0.60 Mn; 0.19 V; 0.07 Nb; Fe – bulk. Material was supplied as a plate thickness of 40 mm produced by the hot rolling with subsequent thermal treatment (TT). Standard thermal treatment included normalization at 1040 °C during 30 minutes with air cooling and subsequent tempering at 730 °C during 60 min with air cooling to room temperature.

The SPD process was carried as follows: the initial cylindrical sample with diameter of 40 mm was extruded at the temperature of 875 °C into the cylinder with the diameter of 20 mm. The resulting sample with diameter of 20 mm and height of 60 mm was subjected to annealing at 1250 °C during 1 h (to dissolve carbides) and then three "upsetting-extrusion" cycles 20 – 30 – 20 mm were carried out at T = 875 °C on hydraulic press DB 2432A with force of 160 tf. The true (logarithmic) strain during one cycle of "upsetting-extrusion" was e ≈1.6 and the total true strain for the 3 cycles was e ≈ 4.8. The extrusion-upsetting process is described in more detail in [24]. Following the SPD process, the samples were subjected to a annealing at temperatures of 550…730 °C during different time. The annealing was carried out in quartz ampoules in an argon environment, followed by air cooling.

Microstructural studies were carried out on metallographic inversion microscope Olympus GX51 and scanning electron microscope JEOL 7001-F. The fine structure of specimens was studied on transmission electron microscope JEM-2110 (accelerating voltage 200 kV) equipped with scanning attachment BF-STEM JEOL EM-24511 and energy dispersion X-ray microanalyzer JEOL EX-24063 JGP. Specimens for metallographic studies were preliminary encapsulated into bakelite and then grinded on SiC paper (graininess from P120 to P1200) and polished on diamond suspensions with fraction size of 1 and 0.05 μm. To reveal the microstructure Vielle`s reagent was used (5 ml of hydrochloric acid, 1 g of picric acid and 100 ml of ethanol). For TEM study plates 0.3 mm thickness were cut out by spark cutting and mechanically thinned to 0.15 mm. The further thinning was carried out by standard jet electropolishing using Tenupol unit at room temperature of electrolyte (electrolyte composition: 80% C_2H_5OH, 10% $HClO_4$, 10% $C_3H_8O_3$, voltage 70 V). Parameters of grain structure and carbide precipitates (mean size d_m and coefficient of size variation k_v of grains and phases) were determined by computer digital treatment of structure images and further data treatment based on the empiric approach in static package SPSS.

X-ray diffraction study was carried out using DRON-2.0 diffractometer in Bragg-Brentano geometry using filtered Co-K_α radiation. Weight fraction of individual phases (in dual-phase samples) was determined by Rietveld refinement (Maud software). Lattice parameters were calculated by least-square fitting. Estimation of microstructural characteristics (crystallite size (CS) D, microstrains ε and dislocations density ρ) is based on diffraction peaks broadening. Analysis was performed by the method proposed in [25]; the main formula is:

$$\beta(s)D = \frac{1}{1-4\varepsilon^2 / d\beta^2(s)}, \quad (1)$$

where β – physical broadening; $s = 2\sin\theta/\lambda = 1/d$; λ – radiation wavelength; θ – diffraction angle; d – interplanar spacing; D – crystallite size; ε – micro-strains. Two orders of diffraction peaks (110) and (220) were used for analysis. Silicon powder was used as reference material for calibration of instrumental broadening. Determining of dislocations density was carried out by the formula:

$$\rho = \frac{3\sqrt{2\pi}\varepsilon}{Db}, \quad (2)$$

where ρ – dislocations density; b – Burgers vector. For BCC metals and alloys Burgers vector defined as $b = \frac{a}{2}<111>$, where a – lattice parameter.

Microhardness tester LM 700 AT was used for Vickers hardness measurements. The measurement conditions are as follows: load – 200 g, holding time – 14 s. The hardness was measured along the entire surface of the sample section from edge to edge. The

minimum number of hardness impress was 10 imprints with a distance of about 4 diagonals of the imprint between them. The measurement error did not exceed 8%. The ImageJ program was used for calculating the density of precipitates. In total, at least 1500 objects were processed on each sample. Mechanical properties of steel T91 (tensile strength σ_B, yield strength σ_τ, elongation δ) were determined by testing of dog-bone specimens with a gage length of 17 mm, width of 2.4 and 0.8 mm thickness at a strain rate of 10^{-3} s^{-1} and temperatures 20 and 600 °C Specimens were cut using the electric spark method and mechanically polished to mirror glance before testing. At each temperature three samples were tested and the measurement results were averaged.

2. RESULTS AND DISCUSSION

2.1. STUDY OF THE MICROSTRUCTURE CHARACTERISTICS

The microstructure of the as-received steel T91 (Fig. 1,a,b) is representative of that observed in tempered martensite, exhibiting the presence of prior austenite grain boundaries and subgrains. These boundaries are decorated by precipitates of $M_{23}C_6$-type carbides, which are a constant feature of steel T91 [21, 24]. The mean dimensions of the prior austenite grains, and subgrains precipitates are ≈20 and ≈5 μm, respectively. Martensitic laths with a transverse dimension of 0.25…0.5 μm are observed within prior austenitic grains. At high magnification, in addition to the relatively large $M_{23}C_6$ carbides, a considerable number of fine precipitates with a diameter of ≤50 nm are observed. These precipitates are consistently classified as MX phases [25–27]. The sizes and densities of the precipitates in the initial sample were 125 nm and $9.3\cdot10^{19}$ m^{-3} for $M_{23}C_6$ and 20 nm and $6.5\cdot10^{19}$ m^{-3} for MX, respectively.

The microstructure of the steel after extrusion of an initial sample from a diameter of 40 mm to a diameter of 20 mm at 875 °C is shown in Fig. 1,c. This temperature is in the two-phase austenite-ferrite region, which lies between the critical points A_{C1} = 818 °C and A_{C3} = 925 °C (see [24]). In other words, extrusion was carried out in the region of metastable austenite. The microstructure shown in Fig. 1,c can be characterized as “defective” or “broken” martensite [24]. The cause of such structure formation may be generation of high number of fine grains (subgrains) in austenite with rather high degree of disorientation during extrusion. At subsequent cooling below martensite start temperature the grain (subgrain) boundaries prevent the formation of “traditional” martensite microstructure. In conclusion, obtained microstructure is more similar to usual “subgrain” microstructure with the mean size of subgrains is ≈150 nm. But the rectangular shape of “subgrains” and high microhardness of specimen (~3900 MPa) testify to martensite nature of formed microstructure (see below for more details). It can be noted that formation of such “defective” martensite was observed during refinement of as-received austenitic grains as the result of thermal cycling [28].

The microstructure of the sample after prior normalization at 1250 °C and the next three cycles of extrusion – upsetting also represents defective martensite (see Fig. 1,d). The average size of martensitic subgrains is 105 nm. After treatment, $M_{23}C_6$ carbides acquire a rounded shape (see Fig. 1,d).

XRD analysis of the initial sample revealed only the diffraction peaks of BCC phase (α-phase, ferrite) with a lattice parameter of $a = 2.8714 \pm 2\cdot10^{-4}$ Å (Fig. 2,a, curve 1). Intensity distribution of ferrite peaks corresponds to the non-textured state. The microstrains was $\varepsilon = 1.21\cdot10^{-3}$, and the dislocation density $\rho_D = 3.3\cdot10^{10}$ cm^{-2}. Selected area electron diffraction (SAED) also revealed only α-phase, but in addition, it permitted the identification of the presence of $M_{23}C_6$ carbides (see Fig. 2,b).

Additionally, retained austenite (γ-phase) with an axial texture <111> in direction of extrusion was also revealed in samples after extrusion and after extrusion +3 UEC at 875 °C (see Fig. 2,a, curve 2). The content of austenite in the sample after extrusion is 19.2 wt.%, and the lattice parameter is $a = 3.591 \pm 2\cdot10^{-3}$ Å. For the sample after 3 UEC (see Fig. 2,a, curve 3), the content of γ-phase in the sample is 6.5 wt.%, and the lattice parameter is $a = 3.591\pm2\cdot10^{-3}$ Å. It is unavoidable that retained austenite will persist in steel during the martensitic transformation, as a portion of it remains in a highly stressed state, impeding the phase transition from austenite to martensite. The martensitic transformation process itself causes this stress, rendering its complete elimination unfeasible. As a result, martensitic heat-resistant steels 9%Cr in the tempered state usually contain 3…13% residual austenite [29]. Additional stresses may arise during high-temperature deformation, which also stabilizes austenite. (Assumption that retained austenite can be mechanically stabilized by residual stresses was considered in [30]). This may be associated with an increased austenite content (19.2 wt.%) after extrusion at 875 °C. A lower concentration of retained austenite (6.5 wt.%) after 3 UEC may be caused by a longer total time the sample is kept in the process of three cycles of upsetting – extrusion at 875 °C, i.e. in the austenite-ferrite region. Note that the amount of residual austenite is also affected by the cooling rate [31].

Let us discuss in more detail what phase state the main phase is in the sample after extrusion and 3 UE cycles – ferritic or martensitic? Unfortunately, identification of the martensitic BCT phase by X-ray diffraction was impossible, since the carbon content in T91 steel (≈ 0.09 wt.%) is insufficient at the given level of resolution to observe the splitting of diffraction lines corresponding to the tetragonal lattice of the martensitic phase. However, increased values of the lattice parameter (2.8737 against 2.8714 Å in the initial tempered martensite) and microstrains ($2.44\cdot10^{-3}$ against $1.21\cdot10^{-3}$) and the high dislocation density (against), as well as the high microhardness (3900 against 2440 MPa) suggest that after normalization at 1250 °C and three cycles of upsetting – extrusion the main phase of the samples is martensitic. It follows from this that the microstructure and properties of steel in this state can be significantly changed by annealing (tempering).

Let us consider the transformation of the structural parameters of the matrix phase and carbide precipitates as a result of severe plastic deformation at 875° C and subsequent annealing (tempering) in various modes (Figs. 3 and 4). The average grain (subgrain) size after 3 UEC is 110 nm. The crystallite size is 47 nm compared to 112 nm in the initial N&T state (see Table on Fig. 4). The $M_{23}C_6$ precipitates in the sample exhibited a decrease in size compared to the as-received sample, reaching 115 nm, while the density increased to $2.3 \cdot 10^{19}$ m^{-3}. The carbides of the MX type are distributed in a non-uniform manner, with the greatest accumulation occurring in the interior of martensitic laths (see Fig. 1,d). The mean size of the MX precipitates was ~16 nm, and the density was $2.9 \cdot 10^{21}$ m^{-3}. Therefore, the preliminary normalization at 1250 °C resulted in the partial dissolution of carbides, which were subsequently re-precipitated during the deformation and the cooling processes.

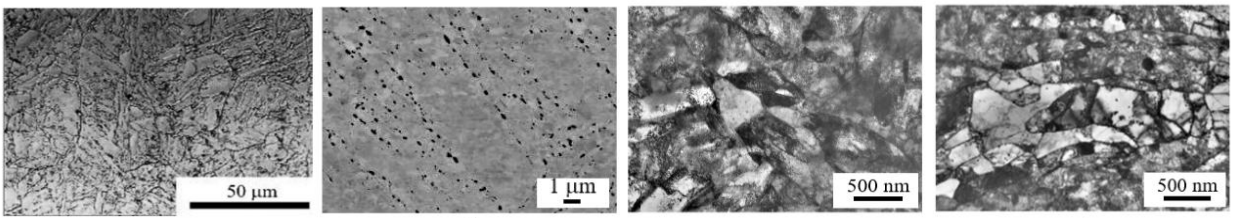

a *b* *c* *d*

Fig. 1. Microstructure of initial T91 (a, b); after extrusion at 875 °C (c); after prior normalization at 1250 °C + 3 MUE at 875 °C (d)

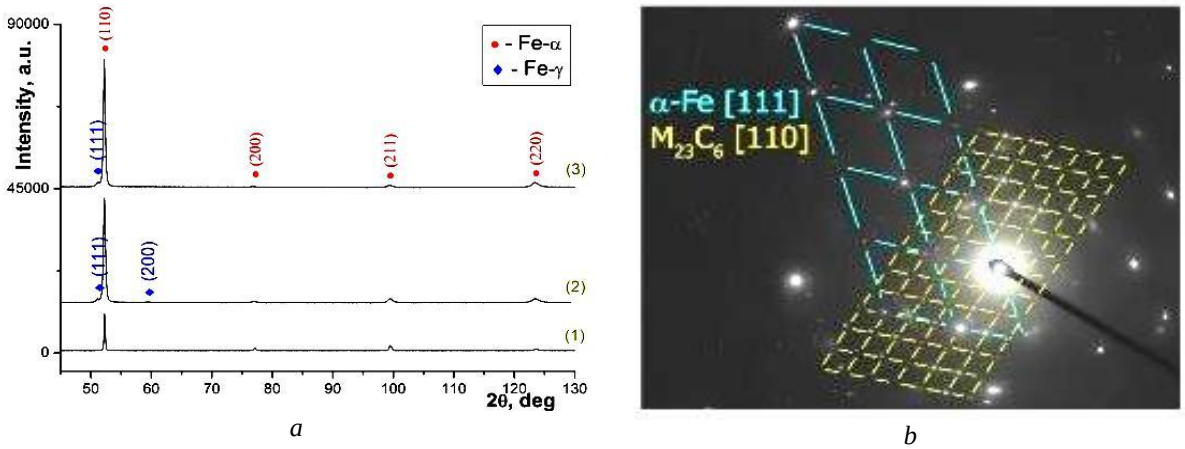

a *b*

Fig. 2. Diffraction patterns of steel T91: a – XRD (1 – initial, 2 – after extrusion at 875 °C, 3 – after prior normalization at 1250 °C + 3 UEC at 875 °C); b – SAED of the initial sample

Following the annealing at 550 °C/25 h, a some diffusion process is initiated, whereby the "broken" martensite in some regions of the sample transforms into a more "classical" form and assembles into blocks, accompanied by an increase in the subgrain size to 173 nm (see Fig. 3,a,b). The mean width of the martensite lamellae is 340 nm. It is notable that a considerable number of secondary phase precipitates are observed in some lamellae. $M_{23}C_6$ carbides are located along the boundaries of martensitic laths and subgrains, and their shape is faceted in some instances. The presence of carbides of the MX type was observed in the grain body and near the boundaries of martensitic laths.

An increase in the annealing temperature to 600 °C results in the continued enlargement of the microstructure, yet the "lamellae + subgrains" structure is still preserved in the sample (see Fig. 3,c,d). The width of the martensitic laths increases to 700 nm, the subgrains growth also continues (up to ~210 nm), but the growth rate is low. $M_{23}C_6$ and MX carbides are enlarged, and some $M_{23}C_6$ carbides also have a faceted shape.

A further increase in the annealing temperature to 650 °C/25 h leads to the onset of recrystallization, to the appearance of recrystallized grains 1.5 μm in size and formation of a bimodal microstructure (see Fig. 3,e). Increasing the annealing temperature to 730 °C sharply increases the recrystallization rate and within only one hour a completely recrystallized microstructure with an average grain size 2.8 μm is formed (see Fig. 3,f). A comparable tendency in the structural changes of T91 steel subsequent to was observed in [32]. The evolution of the microstructure was observed in the a thermomechanically treated T91 steel during thermal holding at 600 °C for 6 h, and particularly strong changes in the microstructure of T91 steel occurred after a short-term annealing at 700 °C.

Diffraction patterns of T91 samples after deformation and subsequent annealing at 550 and 600 °C are presented in Fig. 4. The samples after annealing at these temperatures are single-phase and contain only α-Fe. The intensity distribution of ferrite lines in both samples corresponds to the non-textured state.

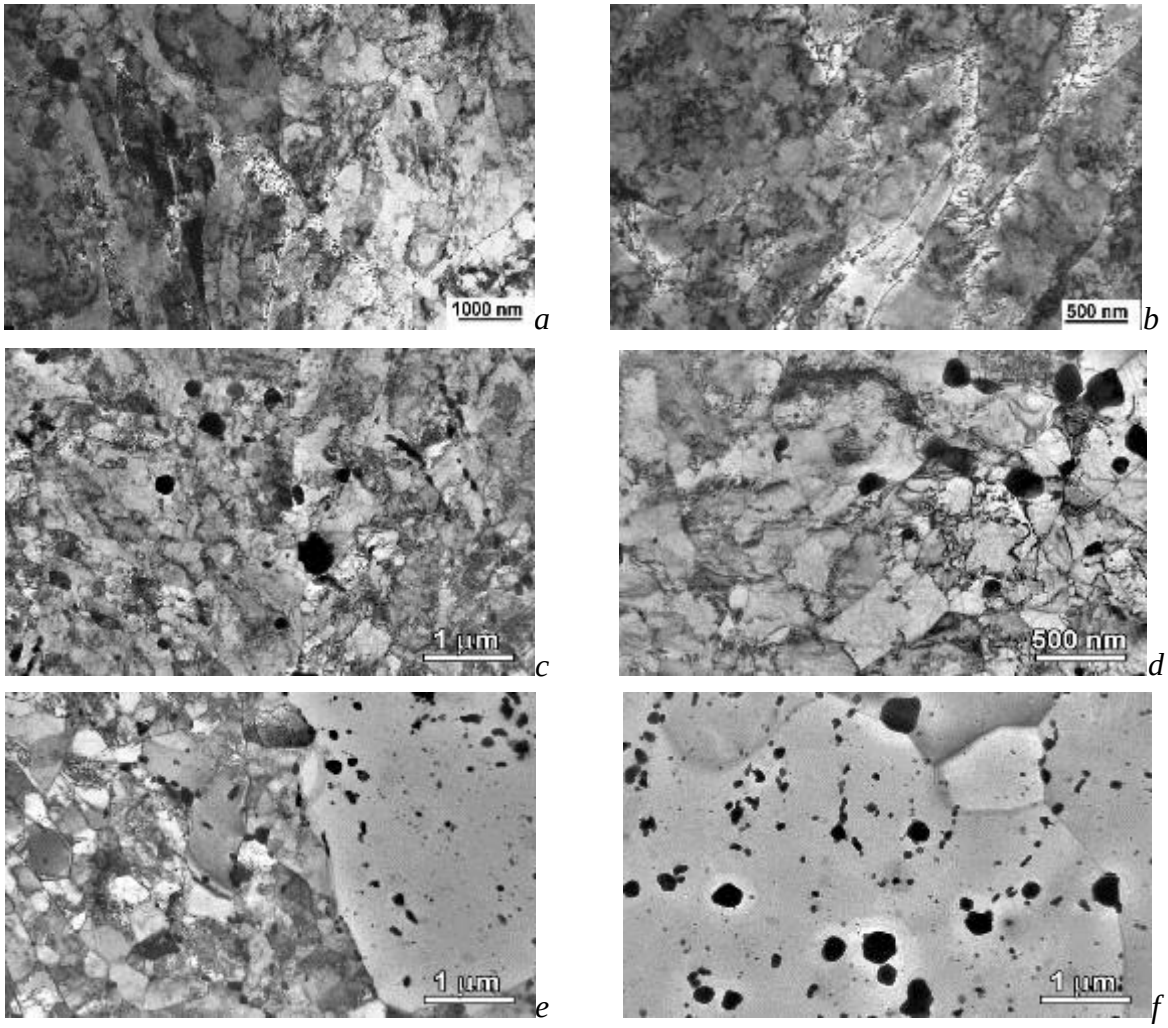

Fig. 3. Microstructure of steel T91 after prior normalization at 1250 °C + 3 UEC at 875 °C and annealing at different temperatures: a, b – 550 °C/25 h; c, d – 600 °C/25 h; e – 650 °C/25 h; f – 730 °C/1 h

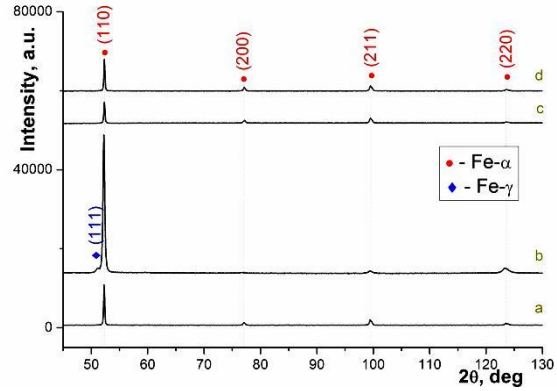

Sample	Phase	Fraction, %wt	Lattice parameter *a*, Å	Microstructural characteristics		
				Crystal-lite size *D*, nm	Micro-strains ε	Dislocations density ρ_D, cm^{-2}
Initial N&T	Fe-α	100	2.8714	111.6	$1.2 \cdot 10^{-3}$	$3.28 \cdot 10^{10}$
Normalization at 1250 °C + 3 UEC	Fe-α	93.5	2.8737	46.9	$2.4 \cdot 10^{-3}$	$15.7 \cdot 10^{10}$
	Fe-γ	6.5	3.591	-	-	-
550°C/24h	Fe-α	100	2.8716	136.9	$2.0 \cdot 10^{-3}$	$4.35 \cdot 10^{10}$
650°C/24h	Fe-α	100	2.8711	150.2	$1.6 \cdot 10^{-3}$	$3.29 \cdot 10^{10}$

Fig. 4. Diffraction pattern of T91 steel: a – initial N&T; b – after normalization at 1250 °C + 3 UEC; c – after annealing at 550 °C/25 h; d – after annealing at 600 °C/25 h. Phase composition and structural characteristics of samples (in Table)

The absence of retained austenite in the samples after annealing is attributed to the fact that in 9% Cr ferritic-martensitic steels, when tempered at 540 °C for at least 45 min, the retained austenite undergoes complete decomposition and transforms into martensite [30, 33, 34].

In comparison to the sample that underwent SPD at 875 °C, the level of microstrains decreased by 1.2 and 1.5 times, respectively, after heat treatment at 550 and 600 °C. Additionally, the crystallite size D increased approximately threefold. In parallel, the dislocation density is observed to decrease by a factor of 3.6 (for annealing at 550 °C/24 h) and 4.8 (for annealing at 600 °C/24 h) in comparison to the sample subjected to 3 UEC.

The distribution of elements in the matrix and precipitates of the steel after 3 UEC at 875 °C is shown in Fig. 5, which presents the results of mapping on an electron microscope. The main steel elements Fe and Cr are uniformly distributed throughout the matrix. The large chromium-rich $M_{23}C_6$ carbide precipitates are apparent by an increase in the intensity of other alloying elements in the steel and therefore have a variable composition of $(Fe, Cr, Mn, Mo, V)_{23}C_6$. These carbides are precipitated during steel tempering, exhibiting usually sizes up to 200 nm and a predominant localization along prior austenite grain boundaries and martensite laths. The presence of strong carbide-forming elements, namely vanadium and niobium, in the steel results in the formation of small carbide precipitates of the MX type at dislocation and lamellae boundaries. Meanwhile, the MX precipitates show a greater enrichment in vanadium and a lesser enrichment in niobium.

Compared to the initial &T state, in the steel after 3 UEC a significantly higher density of MX carbides is observed. At the same time, the average sizes of carbides of both types differ slightly. Approximately the same ratio is observed after annealing at 550 and 600 °C, however, annealing at 650 °C significantly reduces the density of MX carbides and increase the density of $M_{23}C_6$ (Table 1).

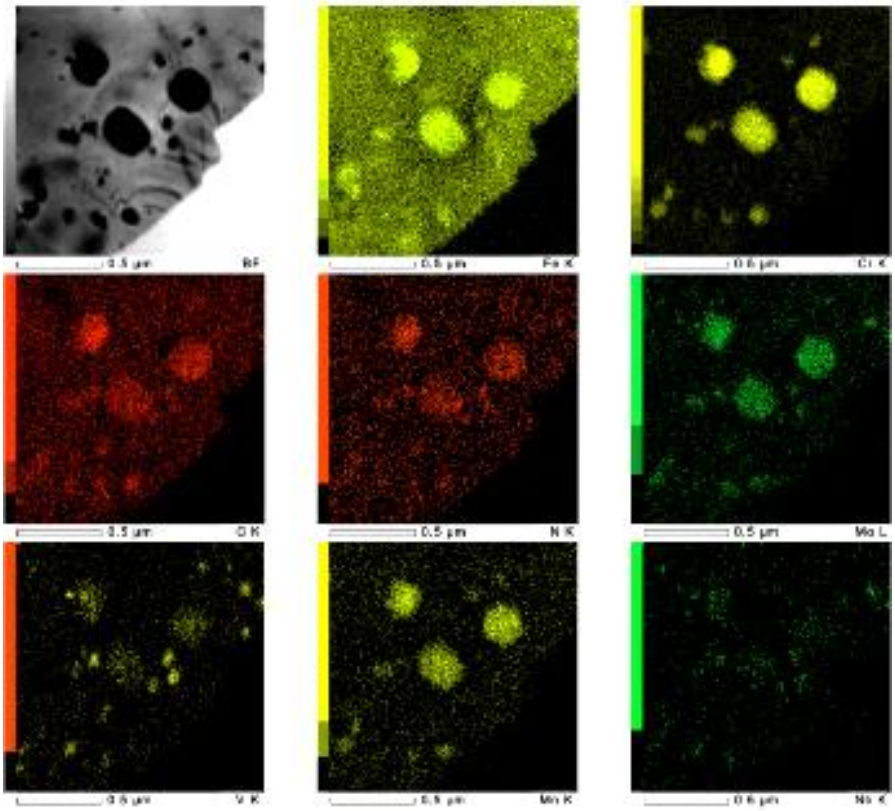

Fig. 5. Distribution of elements in precipitates and matrix of the ferritic-martensitic steel T91 after 3 UEC at 875 °C

Table 1

Microstructure parameters of T91 steel after SPD at 875 °C and annealing at different temperatures
(d_{mg} – mean subgrain size, ρ – precipitates density;
d_{mf} – mean size of precipitates; f_V – precipitates volume fraction)

Sample	d_{mg}, μm	ρ, 1/m^3		d_{mf}, nm		f_V, %	
		$M_{23}C_6$	MX	$M_{23}C_6$	MX	$M_{23}C_6$	MX
Initial N&T	20.00	$9.3\cdot10^{19}$	$6.5\cdot10^{19}$	126	20	7.5	0.3
Normalisation at 1250 °C + 3 UEC	0.11	$2.3\cdot10^{19}$	$2.9\cdot10^{21}$	115	16	1.6	5.9
TT at 550 °C	0.17	$2.7\cdot10^{19}$	$3.8\cdot10^{21}$	81	16	1.0	8.1
TT at 600 °C	0.21	$4.2\cdot10^{19}$	$2.6\cdot10^{21}$	121	20	2.8	5.5
TT at 650 °C	1.5	$7.0\cdot10^{19}$	$2.3\cdot10^{20}$	105	28	6.7	0.7
TT at 730 °C	2.7	–	–	–	–	–	–

The highest density ($3.8 \cdot 10^{21}$ m^{-3}) and the smallest size (16 nm) of MX carbides were identified in the sample subjected to annealing at 550 °C. In comparison with the sample subjected to 3 UCE, the size of MX in the samples after treatment at 550 °C remains constant with a value of 16 nm. An increase in the tempering temperature to 600 °C results in a non-critical reduction in the density of MX precipitates ($2.6 \cdot 10^{21}$ m^{-3}). However, at temperatures of 650 °C, a sharp decrease in the density of MX particles and an increase in their size are observed (see Table 1).

2.2. INVESTIGATION OF MECHANICAL PROPERTIES

The microhardness of T91 steel in its as-received condition, following standard heat treatment in accordance with ASTM A217 [9], was 2480 MPa, which is representative of the typical range for this steel. Following deformation of T91 steel at a temperature of 875 °C, a significant increase in microhardness was observed. This result demonstrates that, according to the phase diagram, during extrusion at 875 °C, the sample is situated within the two-phase stability region of austenite and ferrite. Moreover, the austenite phase constituted the majority, and its transformation into martensite during the cooling of the sample after extrusion resulted in high microhardness values. Furthermore, the dissolution of carbide precipitates and the transition of carbon to a solid solution can contribute to steel hardening due to SPD at 875 °C.

The tempering of the deformed steel should result in the stabilization of the ultra-fine grained microstructure and the release of carbon from the solid solution in the form of carbides, primarily of the MX type, on the substructure elements, namely the boundaries of "broken" martensite and dislocations. Subsequent tempering was conducted at temperatures of 550, 600, and 650 °C for periods of up to 100 h. The results of the studies examining the impact of deformation and subsequent heat treatments on the microhardness of steel T91 are presented in Table 2 and Fig. 6.

Table 2

Microhardness of ferritic-martensitic steel T91 after TMT in the field of austenite stability

Sample	Microhardness, MPa
Initial	2480
Extrusion at 875 °C	3927
Annealing at 1250 °C	3644
Annealing at 1250 °C + 3 MUE	3958
TT at 550 °C	3100
TT at 600 °C	2781
TT at 650 °C	1931

As can be seen from Table 2 and Fig. 6, the deformation carried out in the form of 3 UEC cycles resulted in a notable refinement of the microstructure (see Fig. 1), partial transition of carbon to solid solution, and consequently, an increase in microhardness values to 3958 MPa, which is 1.6 times higher than the value for the initial state (2480 MPa).

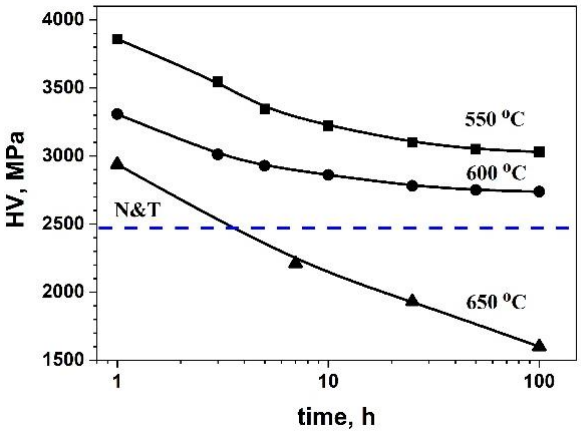

Fig. 6. Changes in microhardness of ferritic-martensitic steel T91 depending on the annealing time at different temperatures

The portion of the carbon that was released into the solid solution during high-temperature deformation cycles is precipitated as carbides. $M_{23}C_6$ undergoes changes in size and density, while nanometer-scale precipitates of the MX type with high density are formed, as evidenced by the results of electron microscopic studies. The formation of carbides inhibits the movement of dislocations and the growth of grains, thereby fixing the ultra-fine grained microstructure. These processes are associated with structural changes that affect microhardness and other mechanical characteristics.

Tempering at 550 °C initially results in a rapid but insignificant loss of hardness. The softening process reaches saturation after 25 h of annealing, and further holding for up to 100 h did not result in any noticeable changes (see Fig. 3,a,b). When annealing at a temperature of 550 °C occurs a significant reduction in microstrains and dislocation density, as well as an increase in the average size of subgrains. These microstructural changes lead to a decrease in microhardness. A similar but more extensive pattern of changes was observed for a tempering temperature of 600 °C. After 25 h of holding, the microhardness reached 2781 MPa and remained constant for 100 h of tempering.

Nevertheless, elevating the tempering temperature to 650 °C leads to pronounced recrystallization, which is further intensified at temperatures exceeding 730 °C. The martensitic microstructure is destroyed, the grain size increases catastrophically, and the density of carbides decreases. These processes are responsible for a notable reduction in microhardness during the tempering of deformed samples.. Therefore, it is recommended that the maximum tempering temperature should not exceed 600 °C.

The mechanical properties of T91 steel were determined under active tensile conditions at temperatures of 20 and 600 °C.

The outcomes of tensile testing on samples subjected to various forms of treatment are presented in Table 3.

As observed in [8, 10], MX-type precipitates effectively pin dislocations and grain subboundaries, thereby enhancing the high-temperature strength of steels and their creep resistance. A direct correlation can be observed between the density of MX precipitates and the resulting strength of the samples, as evidenced by the data presented in Table 1.

Table 3

Yield strength ($\sigma_{0.2}$), ultimate tensile strength (σ_B) and unit elongation (δ) of the ferritic-martensitic steel T91, tested at different temperatures (T_{test})

Sample	T_{test}, °C	$\sigma_{0.2}$, МПа	σ_B, МПа	δ, %
Initial (N&T)	20	728	797	14.5
	600	350	376	16.8
Normalisation at 1250 °C + 3 UEC	20	1279	1340	11,1
	600	502	511	15.6
Tempering at 550 °C / 25 h	20	908	1051	10.2
	600	530	568	14.2
Tempering at 600 °C / 25 h	20	787	875	6.61
	600	381	415	14.1

As can be observed, the strength characteristics of the T91 steel that has undergone severe plastic deformation at 875 C° exhibit a notable enhancement in comparison to those of the steel in its initial state. This difference may be attributed to two factors. Firstly, the difference in the subgrain structure resulting from the application of the SPD technique via the upsetting-extrusion method. Secondly, the presence of hardening carbide precipitates must also be considered. These two factors influence the tensile diagram and strength values at room temperature, as well as at 600 °C in particular.

As previously indicated, tempering at 650 °C results in recrystallization and an increase in the average grain size, despite the presence of carbide precipitates. This process is accompanied by a notable degradation of mechanical properties. Therefore, the upper temperature limit for the materials obtained is 600 °C.

CONCLUSIONS

The impact of severe plastic deformation via the multi-cycle "upsetting-extrusion" method and subsequent thermal treatment on the microstructural changes and mechanical properties of ferritic-martensitic steel T91 was investigated. In accordance with the aforementioned analysis, the following conclusions can be drawn:

1. The application of severe plastic deformation through the method of multiple "upsetting-extrusion" at 875 °C enables the formation of an ultra-fine grained structure in T91 steel, with a minimum grain size of "defective" martensite ~100 nm.

2. The application of thermomechanical treatment to T91 steel at temperatures corresponding to the austenitic – ferritic range permitted the efficient refinement and re-precipitation of secondary phase carbides. The highest density of nanosized MX-type carbides was observed following tempering at 550 °C.

3. The stabilization of the microstructure is facilitated by tempering at 550 and 600 °C. The optimal temperature for tempering is 600 °C for 25 h, resulting in the formation of a stable, fine-grained structure with enhanced mechanical properties.

4. The highest value of the T91 steel microhardness was recorded in the sample after extrusion (3927 MPa), which exceeds the hardness value for the original sample by more than 1.5 times. Following tempering at temperatures of 550 and 600 °C, the hardness remains at a relatively high level; however, a notable decline is observed when tempering is conducted at 650 °C. The substantial drop in hardness is attributed to the recrystallization processes that occur in T91 steel at this temperature.

5. A detailed analysis of the mechanical characteristics of the studied ferritic-martensitic steel has revealed that the stabilization of the structure by carbide nanoscale MX precipitates has resulted in a significant enhancement in high-temperature strength, exhibiting an increase of 1.3 times.

REFERENCES

1. U.S. Department of Energy. A Technology Roadmap for Generation IV Nuclear Energy Systems // *Generation IV International Forum, GIF-002-00*, December 2002.

2. S.M. Goldberg, R. Rosner. *Nuclear reactors: generation to generation*. Cambridge, MA: American Academy of Arts and Sciences, 2011, 29 p.

3. L.K. Mansur, A.F. Rowcliffe, R.K. Nanstad, S.J. Zinkle, W.R. Corwin, R.E. Stoller. Materials needs for fusion, Generation IV fission reactors and spallation neutron sources – similarities and differences // *J. Nucl. Mater.* 2004, v. 329-333, p. 166-172.

4. R. Klueh, D. Harries. *High-Chromium Ferritic and Martensitic Steels for Nuclear Applications*. West Conshohocken: ASTM International, 2001, 221 p.

5. R.L. Klueh, A.T. Nelson. Ferritic/martensitic steels for next-generation reactors // *J. Nucl. Mater.* 2007, v. 371, issue 1-3, p. 37-52.

6. C. Cabet, F. Dalle, E. Gaganidze, J. Henry, H. Tanigawa. Ferritic-martensitic steels for fission and

fusion applications // *J. Nucl. Mater*. 2019, v. 523, p. 510-537.

7. T. Jayakumar, M.D. Mathew, K. Laha. High temperature materials for nuclear fast fission and fusion reactors and advanced fossil power plants // *Procedia Eng*. 2013, v. 55, p. 259-270.

8. R.L. Klueh. Elevated temperature ferritic and martensitic steels and their application to future nuclear reactors // *Int. Mater. Rev*. 2005, v. 50, issue 5, p. 287-310.

9. https://www.astm.org/a0213_a0213m-18.html

10. K. Maruyama, K. Sawada, J. Koike Strengthening Mechanisms of Creep Resistant Tempered Martensitic Steel // *ISIJ International*. 2001, v. 41, N 6, p. 641-653.

11. T. Shrestha et al. Effect of heat treatment on microstructure and hardness of Grade 91 steel // *Metals*. 2015, v. 5, p. 131-149.

12. P.J. Ennis et al. Influence of heat treatments on microstructural parameters and mechanical properties of P92 steel // *Mater. Sc. and Techn.* 2000, v. 16, issue 10, p. 1226-1233.

13. S. Raju, B.J. Ganesh, A. Kumar, et al. Measurement of transformation temperatures and specific heat capacity of tungsten added reduced activation ferritic–martensitic steel // *J. Nucl. Mater*. 2009, v. 389, p. 385-393.

14. K.S. Chandravathi, C.S. Sasmal, K. Laha, P. Parameswaran, et al. Effect of isothermal heat treatment on microstructure and mechanical properties of reduced activation ferritic martensitic steel // *J. Nucl. Mater*. 2013, v. 435, p. 128-136.

15. L. Huang, X. Hu, C. Yang, W. Yan, F. Xiao, Y. Shan, K. Yang. Influence of thermal aging on microstructure and mechanical properties of CLAM steel // *J. Nucl. Mater*. 2013, v. 443, p. 479-483.

16. C. Sun, M. Song, K. Yu, Y. Chen, M. Kirk, M Li, H. Wang, X. Zhang. In situ evidence of defect cluster absorption by grain boundaries in Kr ion irradiated nanocrystalline Ni // *Metall. Mater. Trans. A*. 2013, v. 44, p. 1966-1974.

17. P. Fernández et al. Microstructural and mechanical characteristics of EUROFER'97 processed by equal channel angular pressing // *J. Nucl. Mater*. 2011, v. 417, p. 20-24.

18. M. Song et al. A roadmap for tailoring the strength and ductility of ferritic/martensitic T91 steel via thermo-mechanical treatment // *Acta Mater*. 2016, v. 112, p. 361-377.

19. S.S. Samant et al. Influence of intermediate rolling on mechanical behavior of modified 9Cr-1Mo steel // *Mater. Sci. Eng. A*. 2018, v. 738, p. 135-152.

20. S. Hollner, B. Fournier, J. Le Pendu, T. Cozzika, et al. High-temperature mechanical properties improvement on modified 9Cr-1Mo martensitic steel through thermomechanical treatments // *J. Nucl. Mater*. 2010, v. 405, p. 101-105.

21. J. Vivas, C. Capdevila, J.A. Jimenez, M. Benito-Alfonso, D. San-Martin. Effect of Ausforming Temperature on the Microstructure of G91 Steel // *Metals*. 2017, v. 7, p. 236.

22. J. Hoffmann et al. Improvement of reduced activation 9%Cr steels by ausforming // *Nucl. Mater. Energy*. 2016, v. 6, p. 12-17.

23. A. Chatterjee, D. Chakrabarti, A. Moitra, R. Mitra, A.K. Bhaduri. Effect of deformation temperature on the ductile-brittle transition behavior of a modified 9Cr-1Mo steel // *Mater. Sci. Eng. A.* 2015, v. 630, p. 58-70.

24. V.N. Voyevodin, M.A. Tikhonovsky, H.Yu. Rostova, A.S. Kalchenko, I.V. Kolodiy, N.F. Andrievskaya, V.S. Okovit, M. Serrano, R. Hernandez, O.M. Velikodnyi, A.V. Levenets. A new approach to thermo-mechanical treatment of steel T91 by multiple upsetting-extrusion in a ferritic range // *Materials Science and Engineering: A*. 2021, v. 822, p. 141686;
https://doi.org/10.1016/j.msea.2021.141686

25. H.P. Klug, L.E. Alexander. *X-ray Diffraction Procedures for Polycrystalline and Amorphous Materials*. 2nd Edition, New York: John Wiley & Sons, 1974, 992 p.

26. M. Tamura, H. Hayakawa, M. Tanimura, A. Hishinuma, T. Kando. Development of potential low activation ferritic and austenitic steels // *J. Nucl. Mater.* 1986, v. 141-143, p. 1067-1073.

27. M. Tamura, K. Ikeda, H. Esaka, K. Shinozuka. Precipitation behavior of NbC in 9%Cr1%Mo0.2%VNb steel // *ISIJ Int.* 2001, v. 41, p. 908-914.

28. B.J. Hidalgo, M.S. Santofimia. Effect of prior austenite grain size refinement by thermal cycling on the microstructural features of as-quenched lath martensite // *Metall. Mater. Trans. A.* 2016, v. 47A, N 11, p. 5288-5301.

29. D.A. Carrizo, J.I. Besoky, M. Luppo, C. Danon, C.P. Ramos. Characterization of an ASTM A335 P91 ferritic-martensitic steel after continuous cooling cycles at moderate rates // *J. Mater. Res. Technol.* 2019, v. 8, issue 1, p. 923-934.

30. R.K. Shiue, K.C. Lan, C. Chen. Toughness and austenite stability of modified 9Cr–1Mo welds after tempering // *Mater. Sci. Eng. A*. 2000, v. 287, p. 10-16.

31. M. Ni, J. Wang, J. Liu, et al. Microstructure and Mechanical Properties of P91 Steel during Heat Treatment: The Effect of the Cooling Speed during the Normalization Stage // *J. Mater. Eng. and Perform.* 2021, v. 30, p. 2329-2340.

32. E. Oñorbe, M. Hernández-Mayoral, R. Hernández, M. Serrano. Microstructural study of the thermal stability of a thermomechanically treated T91 steel by TEM in situ annealing // *Nucl. Mater. Energy*. 2022, v. 32, p. 101213.

33. X. Tao, C. Li, L. Han, J. Gu. Microstructure evolution and mechanical properties of X12CrMoWVNbN10-1-1 steel during quenching and tempering process // *J. Mater. Res. Technol.*, 2016, v. 5, issue 1, p. 45-57.

34. Y. Zhang, J. Gu, L. Han, G. Shen, C. Li. Thermal decomposition characteristics of retained austenite and its influence on impact toughness of B-containing 9Cr1Mo1Co(FB2) steel during the two-step tempering // *J. Mater. Res. Technol.* 2021, v. 12, p. 2462-2475..

Article received 06.08.2024

ВПЛИВ ІНТЕНСИВНОЇ ПЛАСТИЧНОЇ ДЕФОРМАЦІЇ ПРИ ВИСОКИХ ТЕМПЕРАТУРАХ НА МІКРОСТРУКТУРУ ТА МЕХАНІЧНІ ВЛАСТИВОСТІ ФЕРИТНО-МАРТЕНСИТНОЇ СТАЛІ Т91

Г.Ю. Ростова, І.В. Колодій, Р.Л. Василенко, О.С. Кальченко, М.А. Тихоновський, О.М. Великодний, Г.Д. Толстолуцька, В.С. Оковіт

Досліджено мікроструктуру та механічні властивості феритно-мартенситної сталі Т91 після інтенсивної пластичної деформації (ІПД) та подальшого відпалу (відпуску). ІПД сталі Т91 проводили методом багаторазової «осадки-екструзії» при температурі 875 °С, подальший відпал проводили в інтервалі температур 550...650 °С протягом 1…100 год. Встановлено, що багаторазовий процес «осадка-екструзія» дозволяє сформувати наддрібнозернисту структуру із середнім розміром зерен біля 100 нм, яка залишається стабільною при температурах відпалу 550 і 600 °С протягом 100 год. Після відпалу при цих температурах мікротвердість залишається на рівні 3100 та 2780 МПа відповідно, що помітно вище, ніж при стандартній термічній обробці цієї сталі (2480 МПа). Зменшення розміру та рівномірний розподіл виділень карбіду типу МХ за рахунок сильної пластичної деформації також призводить до підвищення міцнісних характеристик під час випробувань на розтягування при температурах 20 і 600 °С.